Weak-chaos ratchet accelerator

Itzhack Dana and Vladislav B. Roitberg

Minerva Center and Department of Physics, Bar-Ilan University, Ramat-Gan 52900, Israel
(Received 22 February 2011; published 29 June 2011)

Classical Hamiltonian systems with a mixed phase space and some asymmetry may exhibit chaotic ratchet effects. The most significant such effect is a directed momentum current or acceleration. In known model systems, this effect may arise only for sufficiently strong chaos. In this paper, a Hamiltonian ratchet accelerator is introduced, featuring a momentum current for arbitrarily weak chaos. The system is a realistic, generalized kicked rotor and is exactly solvable to some extent, leading to analytical expressions for the momentum current. While this current arises also for relatively strong chaos, the maximal current is shown to occur, at least in one case, precisely in a limit of arbitrarily weak chaos.

I. INTRODUCTION

Classical [1–6] and quantum [3,6–12] Hamiltonian ratchets have attracted considerable theoretical interest during the past decade. In addition, several kinds of quantum ratchets have been experimentally realized using atom-optics methods with cold atoms or Bose-Einstein condensates [13–16]. The classical Hamiltonian ratchet effect is a directed current in the chaotic region generated by an unbiased force (having zero mean in space and/or time) and due to some spatial and/or temporal asymmetry [1–6]. This is analogous to the ordinary ratchet effect [17,18], but with deterministic chaos replacing the usual noisy environment. Dissipation, an important ingredient in ordinary ratchets for breaking time-inversion symmetry, is absent in Hamiltonian ratchets.

A well-studied class of systems are those described by time-periodic Hamiltonians $H(x,p,t)$ for which both the force $F = -\partial H/\partial x$ and the velocity $v = \partial H/\partial p$ are periodic in x and F has zero mean over (x,t). The classical ratchet current is usually defined as the average of v over (x,p,t), where (x,p) is restricted to the chaotic region; see, e.g., Refs. [2,3]. It is assumed that v is bounded, e.g., by Kolmogorov-Arnol'd-Moser (KAM) tori. Then, necessary conditions for the ratchet current to be nonzero are the breaking of some symmetry and a mixed phase space featuring transporting stability islands that propagate in the x direction [3]. In the presence of bounding KAM tori, one can get, in principle, a nonzero ratchet current also in near-integrable regimes, corresponding to relatively weak and local chaos.

A different and much more significant Hamiltonian ratchet effect was discovered in work [6] for generalized kicked-rotor systems satisfying the well-known KAM scenario. Namely, for sufficiently strong kicking, there exist no KAM tori bounding the chaotic motion in the momentum (p) direction and one thus gets strong global chaos. In addition, transporting accelerator-mode islands [19] propagating in the p direction may arise. This can lead, under some asymmetry conditions, to a ratchet acceleration, i.e., a nonzero mean momentum velocity (rather than the usual position velocity v) of the global chaotic region [6] (see Sec. II for more details). Quantum analogs of the classical ratchet acceleration were found in several systems [9–12], either for special, quantum-resonance values of a scaled Planck constant $\hbar$ [9–11] or for generic values

of $\hbar$ [12]. Quantum-resonance ratchet accelerators have been experimentally realized in recent works [14,15].

In this paper we show that the phenomenon of ratchet acceleration is not limited to strong-chaos regimes. We introduce a realistic Hamiltonian system exhibiting this phenomenon most significantly in near-integrable regimes, corresponding now to arbitrarily weak but global chaos. The system is a generalized kicked rotor whose force function has zero mean and is characterized by two nonintegrability parameters b_1 and b_2. A global chaotic region in the p direction arises also for arbitrarily small values of these parameters, i.e., the KAM scenario is not satisfied. As $b_1,b_2 \to 0$, this non-KAM [20] system tends to the well-known elliptic sawtooth map [21,22], which has been used as a paradigmatic model of pseudochaos (dynamical complexity with a zero Lyapunov exponent) [22,23] in studies of both classical [22,24] and quantum [25] systems. We show that accelerator-mode islands exist for arbitrarily small b_1 and b_2. Then, when the system is asymmetric ($b_1 \neq b_2$), a ratchet acceleration A may arise for arbitrarily weak chaos. In one particular case, we derive analytical expressions for A as a function of b_1 and b_2. Paths of maximal A in the (b_1,b_2) parameter space are determined. We then show that, in sharp contrast with the systems considered in work [6], A is most significant for relatively small Lyapunov exponents and that its maximal value is attained precisely in a limit $b_1,b_2 \to 0$ of arbitrarily weak chaos.

This paper is organized as follows. In Sec. II we give a short background on Hamiltonian ratchet accelerators. In Sec. III we introduce our general model system and describe its basic properties. In particular, in Sec. III C we derive the existence conditions for the main accelerator-mode islands of the system. In Sec. IV analytical expressions for the ratchet acceleration A in one case are obtained for all values of the parameters. In Sec. V we show that the maximal value of A is attained in a limit of arbitrarily weak chaos. Conclusions are presented in Sec. VI. Detailed derivations of several analytical results are given in the Appendixes.

II. BACKGROUND ON HAMILTONIAN RATCHET ACCELERATORS

The concept of the Hamiltonian ratchet accelerator was introduced in Ref. [6] by adaptation of a formalism developed

in Refs. [2,3]. We give here a self-contained summary of these works, leading to the main result [Eq. (6) below], a sum rule for the ratchet acceleration A. We shall focus on realistic models, the generalized kicked-rotor systems with scaled Hamiltonian $H = p^2/2 + KV(x,t)\sum_{s=-\infty}^{\infty}\delta(t-s)$, where K is the nonintegrability parameter and the potential $V(x,t)$ is periodic in x, $V(x+1,t) = V(x,t)$. Particular cases of these systems were considered in Ref. [6]. The map for H from $t = s - 0$ to $s + 1 - 0$ is given by

$$M: \quad p_{s+1} = p_s + Kf_s(x_s), \quad x_{s+1} = x_s + p_{s+1}\mathrm{mod}(1), \tag{1}$$

where the force function $f_s(x) = -dV(x,t=s)/dx$. Because of the periodicity of $V(x,t)$ in x, $f_s(x)$ satisfies the ratchet (zero-flux) condition: $\langle f_s(x)\rangle = \int_0^1 f_s(x)dx = 0$. As in Ref. [6], we shall assume that the kicking parameter K is large enough that all the rotational (horizontal) KAM tori are broken. Thus there are no barriers to motion in the p direction, leading to a global and strongly chaotic region. These barriers cannot exist if there are accelerator modes, i.e., orbits that are periodic under the map in Eq. (1) in the following sense:

$$p_{s+m} = p_s + w, \quad x_{s+m} = x_s, \tag{2}$$

where m is the period and w, the winding number, is an nonzero integer. Periodic orbits can be defined in the generalized way of Eq. (2) ($w \neq 0$) due to the obvious periodicity of the map in Eq. (1) in p with period 1. If an accelerator mode is linearly stable, each of its points (x_s, p_s) will usually be surrounded by an island $\mathcal{I}_s$, an accelerator-mode island (AMI). Because of Eq. (2), $\mathcal{I}_{s+m}$ is just $\mathcal{I}_s$ translated by w in the p direction. For arbitrary initial conditions $\mathbf{z}_0 = (x_0, p_0)$ in phase space, the mean acceleration (momentum current or velocity) in n iterations of the map in Eq. (1) is

$$A_n(\mathbf{z}_0) = \frac{p_n - p_0}{n} \tag{3}$$

and the average of Eq. (3) in some region $\mathcal{R}$ with area $S_{\mathcal{R}}$ is

$$\langle A_n\rangle_{\mathcal{R}} = \frac{1}{S_{\mathcal{R}}}\int_{\mathcal{R}} A_n(\mathbf{z}_0)\,d\mathbf{z}_0. \tag{4}$$

In the case that $\mathcal{R}$ is an AMI $\mathcal{I}$ with winding number w, it follows from Eqs. (2)–(4) that

$$\lim_{n\to\infty}\langle A_n\rangle_{\mathcal{I}} = \nu = \frac{w}{m}. \tag{5}$$

Now, because of the periodicity of the map [Eq. (1)] in p with period 1, one can also take p_{s+1} modulo (1) in Eq. (1), leading to a map $\bar{M}$ on the unit torus $\mathbb{T}^2$: $0 \leqslant x,\ p < 1$; this is the unit cell of periodicity of the map in Eq. (1). The reduced phase space $\mathbb{T}^2$ can be fully partitioned into the global chaotic region $\mathcal{C}$ with area $S_{\mathcal{C}}$ and all the stability islands $\mathcal{I}^{(j)}$ with areas S_j, where j labels the island: $S_{\mathcal{C}} + \sum_j S_j = 1$. The average acceleration [Eq. (5)] of $\mathcal{I}^{(j)}$ is $\nu_j = w_j/m_j$, where $\nu_j = 0$ for a normal (nonaccelerating) island. We then have the following sum rule relating ν_j to the ratchet acceleration $A = \langle A\rangle_{\mathcal{C}} = \lim_{n\to\infty}\langle A_n\rangle_{\mathcal{C}}$ of the global chaotic region:

$$S_{\mathcal{C}}A + \sum_j S_j \nu_j = 0. \tag{6}$$

Equation (6) is easily derived from the obvious relation $\langle A_n\rangle_{\mathbb{T}^2} = S_{\mathcal{C}}\langle A_n\rangle_{\mathcal{C}} + \sum_j S_j \langle A_n\rangle_{\mathcal{I}^{(j)}}$ by taking $n \to \infty$ and using $\langle A_n\rangle_{\mathbb{T}^2} = 0$, a result following straightforwardly from the map in Eq. (1):

$$\langle A_n\rangle_{\mathbb{T}^2} = \left\langle \sum_{s=1}^{n}\frac{p_s - p_{s-1}}{n}\right\rangle_{\mathbb{T}^2} = \frac{K}{n}\sum_{s=0}^{n-1}\int_{\mathbb{T}^2}d\mathbf{z}_0 f_s(x_s)$$

$$= \frac{K}{n}\sum_{s=0}^{n-1}\int_{\mathbb{T}^2}d\mathbf{z}_s f_s(x_s) = 0, \tag{7}$$

where we used area preservation ($d\mathbf{z}_0 = d\mathbf{z}_s$), the invariance of $\mathbb{T}^2$ under $\bar{M}$, and the ratchet condition $\langle f_s(x)\rangle = 0$. An immediate consequence of the sum rule in Eq. (6) is that A vanishes if the map in Eq. (1) is invariant under inversion, $(x, p) \to (-x, -p)$, i.e., one has the inversion (anti)symmetry $f_s(-x) = -f_s(x)$. This is because under this symmetry for each AMI with mean acceleration $\nu_j \neq 0$ there exists an AMI with the same area but with mean acceleration $-\nu_j$. As we shall see in the following sections for a simple case of $f_s(x)$, A is generally nonzero when AMIs are present and inversion symmetry is absent.

III. GENERAL MODEL SYSTEM AND ITS BASIC PROPERTIES

A. General

The general model system introduced and studied in this paper is the generalized kicked-rotor system described by a simple map in Eq. (1):

$$M: \quad p_{s+1} = p_s + Kf(x_s), \quad x_{s+1} = x_s + p_{s+1}\mathrm{mod}(1), \tag{8}$$

where $0 < K < 4$ and, for $0 \leqslant x < 1$,

$$f(x) = \begin{cases} l_1 x & \text{for } 0 \leqslant x \leqslant b_1, \\ c - x & \text{for } b_1 < x < 1 - b_2, \\ l_2(x-1) & \text{for } 1 - b_2 \leqslant x < 1, \end{cases} \tag{9}$$

with $f(x + 1) = f(x)$. Here b_1 and b_2 are positive parameters with $b_1 + b_2 < 1$ while l_1, l_2, and c, also positive, are fixed by requiring $f(x)$ to be continuous and to satisfy the ratchet condition $\int_0^1 f(x)dx = 0$ (see Appendix A):

$$l_1 = \frac{(1-b_1)(1-b_1-b_2)}{b_1(2-b_1-b_2)}, \quad l_2 = \frac{(1-b_2)(1-b_1-b_2)}{b_2(2-b_1-b_2)},$$

$$c = \frac{1-b_2}{2-b_1-b_2}. \tag{10}$$

Kicked systems with a smooth piecewise linear force function such as Eq. (9) have been studied either on the phase plane [26] or on a cylindrical phase space [27], corresponding to the very special case of the map in Eq. (8) with $b_1 = b_2 = 1/4$. Apparently, however, these systems have not yet been considered in the context of Hamiltonian ratchet transport, i.e., for general values of b_1 and b_2 with $b_1 \neq b_2$, leading to an asymmetric force function in Eq. (9). This general system is realistic since it may be experimentally realized using, e.g., optical analogs as proposed in Ref. [26]. As we shall see

below, the system generally does not satisfy the KAM scenario assumed in Sec. II, i.e., it is a non-KAM system.

B. Phase space and limit cases

The phase space of the map [Eq. (8)] in the basic periodicity torus $\mathbb{T}^2$ ($0 \leqslant x, p < 1$) is illustrated in Fig. 1 for some values of the parameters. We clearly see in all cases a connected chaotic region encircling $\mathbb{T}^2$ in both the x and p directions, implying global chaos and the nonexistence of KAM tori bounding p. An understanding of this numerical observation will be achieved here and in Sec. III C. We first consider here the map in Eq. (8) in the limit of $b_1, b_2 \to 0$. From Eqs. (10) one has $l_1 b_1, l_2 b_2, c \to 1/2$ in this limit, so that the function in Eq. (9) tends to the sawtooth

$$f(x) = 1/2 - x \ (0 \leqslant x < 1), \quad f(x+1) = f(x), \quad (11)$$

with discontinuity at $x = 0$. The map in Eq. (8) with Eq. (11) and $0 < K < 4$ is the well-known elliptic sawtooth map (ESM) [21,22,24,25] having the property that its linearization
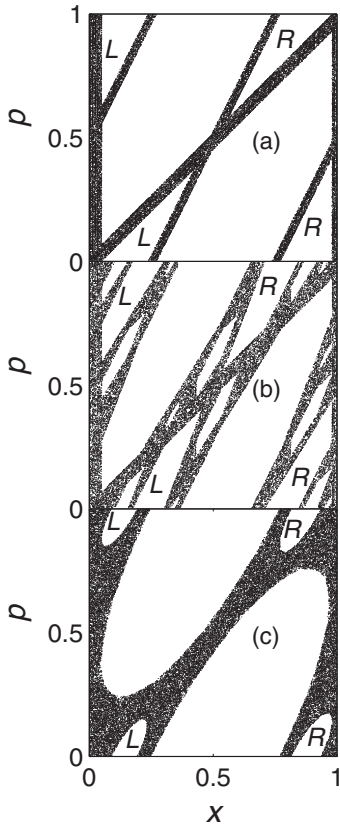

FIG. 2. Global pseudochaotic regions of the ESM for the same values of α (or K) as in Fig. 1. In practice, these regions were generated by iterating a large initial ensemble using the map in Eq. (8) with very small $b_1 = b_2 = 10^{-7}$. The initial ensemble uniformly covered the vertical hyperbolic strip in Eq. (13). The left and right AMIs are again indicated.

DM is a constant 2×2 matrix with eigenvalues $\lambda_\pm$ on the unit circle:

$$\lambda_\pm = \exp(\pm i\alpha), \quad 2\cos(\alpha) = 2 - K. \quad (12)$$

This means that orbits of the ESM that do not cross the discontinuity line $x = 0$ lie on ellipses with average rotation angle α. In general, however, an orbit will cross the $x = 0$ line. Then the combination of the mod(1) operation in Eq. (8) with the local ellipticity of the ESM will usually lead to a complex dynamics with zero Lyapunov exponent, known as pseudochaos [22]. The phase space generally consists of the pseudochaotic region, associated with all iterates of the discontinuity line [21], and a set of islands. More specifically, one has to distinguish between three main cases of the ESM, illustrated in Fig. 2 for the same values of K as in Fig. 1: (a) the integrable case of integer $K = 1, 2, 3$ [corresponding to $\alpha/2\pi = 1/6, 1/4, 1/3$ in Eq. (12)], in which no pseudochaos arises and the phase space consists just of a finite number of separatrix lines (iterates of the discontinuity line) bounding a finite number of islands [see Fig. 2(a)]; (b) the case of noninteger K with rational $\alpha/2\pi$ in Eq. (12), in which numerical work [21] indicates that one has an infinite set of islands and that the pseudochaotic region is a fractal with zero area (see Fig. 2(b) and exact results for the fractal dimension of such regions in other maps with discontinuities [23]); (c) the case of irrational $\alpha/2\pi$, in which one typically has again an infinite set of islands but the pseudochaotic region appears numerically to cover a finite area [21] [see Fig. 2(c)]. Since the momentum p assumes all values on the discontinuity line

FIG. 1. Global chaotic regions of the map [Eq. (8)] within the unit torus of periodicity $0 \leqslant x, p < 1$ for $b_1 = 0.05, b_2 = 0.02$, and three values of K corresponding to the following values of α in Eq. (12): (a) $\alpha = 2\pi/3$ ($K = 3$); (b) $\alpha = 6\pi/5$ ($K \approx 3.618$); and (c) $\alpha = \pi(\sqrt{5} - 1)/2$ ($K \approx 2.7247$). These values of α represent the three main cases discussed in the text. The left (L) and right (R) period-1 accelerator-mode islands (AMIs), see Sec. III C, are indicated in each case.
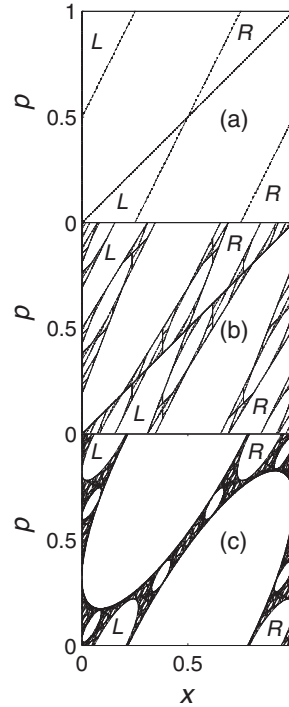
and is thus unbounded, the pseudochaos [or the separatrix in case (a)] is global.

For finite and small b_1 and b_2, the continuous map in Eq. (8) may be considered as a perturbed ESM, with the discontinuity line replaced by a vertical strip B of width $b_1 + b_2$ in $\mathbb{T}^2$ (see also the caption of Fig. 2):

$$B : 0 \leqslant p \leqslant 1, \quad 0 \leqslant x \leqslant b_1 \quad \text{or} \quad 1 - b_2 \leqslant x < 1. \quad (13)$$

This should be contrasted with the perturbed ESM in Ref. [24] for which the discontinuity line is not removed by the perturbation. The linearization DM of Eq. (8) is again a constant 2×2 matrix in each of the three intervals in Eq. (9). In the middle interval, it is the same matrix as for the ESM, with stability eigenvalues [Eq. (12)]. In the other two intervals, where the strip in Eq. (13) is located, DM can be easily shown to have real positive eigenvalues $\lambda_\pm$ with, say, $\lambda_+ > 1$ and $\lambda_- = \lambda_+^{-1} < 1$, i.e., there is local hyperbolicity. One can then expect that already for small b_1 and b_2 a global chaotic region with a positive Lyapunov exponent will emerge from the vertical strip in Eq. (13) and will replace the global pseudochaos (or separatrix) for $b_1 = b_2 = 0$. This can be clearly seen by comparing Figs. 1 and 2. The nature of the chaotic region will be discussed further in the following sections, where it will be shown numerically that the Lyapunov exponent indeed tends to zero as $b_1, b_2 \to 0$.

C. Accelerator-mode islands and their existence conditions

We show here that AMIs for the map in Eq. (8) rigorously exist in broad ranges of the parameters, including arbitrarily small values of b_1 and b_2. This exactly implies global and arbitrarily weak chaos. We shall consider only period-1 AMIs, associated with stable accelerator modes satisfying Eq. (2) with $m = 1$ and $w \neq 0$. As we shall see, there appear to be no higher-period AMIs at least in the case of $K = 3$ on which we shall focus from Sec. IV on. The initial conditions (x_0, p_0) for $m = 1$ stable periodic orbits in Eq. (2) must necessarily lie in the middle interval in Eq. (9), $b_1 < x_0 < 1 - b_2$, since only in this interval the matrix DM exhibits stability eigenvalues [Eq. (12)]. Thus, from Eqs. (2), (8), and (9), we get

$$x_0 = c - \frac{w}{K}, \quad p_0 = 0 \bmod(1), \quad (14)$$

$$b_1 < c - \frac{w}{K} < 1 - b_2. \quad (15)$$

For $w = 0$ one has a nonaccelerating stable fixed point ($x_0 = c, p_0 = 0$), the center of a normal (nonaccelerating) island. We show that w may take only two nonzero values and this only in some interval of K:

$$w = \pm 1, \quad 2 \leqslant K < 4. \quad (16)$$

In fact, from Eqs. (9) and (10) it follows that the maximal value of $|f(x)|$ is $\max(l_1 b_1, l_2 b_2) < 1/2$. Then, since $w = K f(x_0)$ from Eqs. (2) and (8), we have $|w| \leqslant [K/2]$, where [ ] denotes the integer part. This implies, for $0 < K < 4$, that w may take the only nonzero values of ± 1 provided $2 \leqslant K < 4$.

Now, according to Eq. (14) for x_0, the values of $w = 1$ and -1 should correspond, respectively, to a left (L) and a right (R) AMI (see Figs. 1 and 2). An explicit existence condition
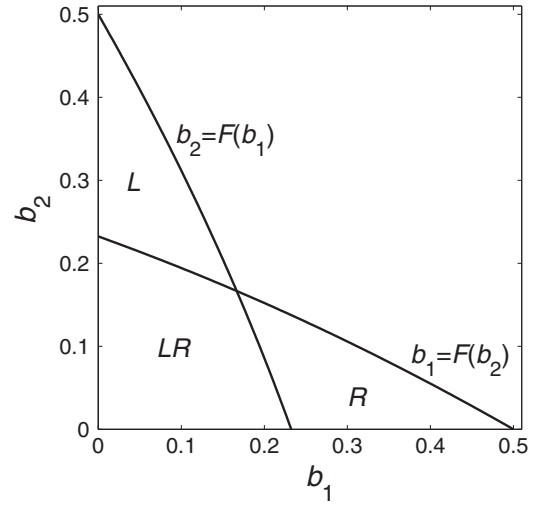

FIG. 3. Curves $b_2 = F(b_1)$ and $b_1 = F(b_2)$ [with $F(b_1)$ given by Eq. (17) for $K = 3$] defining the domains of existence of the left and right period-1 AMI for $K = 3$ in the (b_1, b_2) plane. In domain L (R), only the left (right) AMI exists. In domain LR, both AMIs exist. No AMIs exist elsewhere.

for the left AMI ($w = 1$) is derived, after some simple algebra, from the left inequality in Eq. (15) using Eq. (10) for c:

$$b_2 < F(b_1) \equiv \frac{K b_1^2 + (1 - 2K) b_1 + K - 2}{K - 1 - K b_1} \quad (17)$$

(see also note [28]). It is easily verified that the right inequality in Eq. (15) is identically satisfied. Similarly, the existence condition for the right AMI is $b_1 < F(b_2)$. One thus has three cases (compare with Fig. 3 for $K = 3$).

(a) Both AMIs L and R exist (see, e.g., Figs. 1 and 2) if

$$b_2 < F(b_1), \quad b_1 < F(b_2). \quad (18)$$

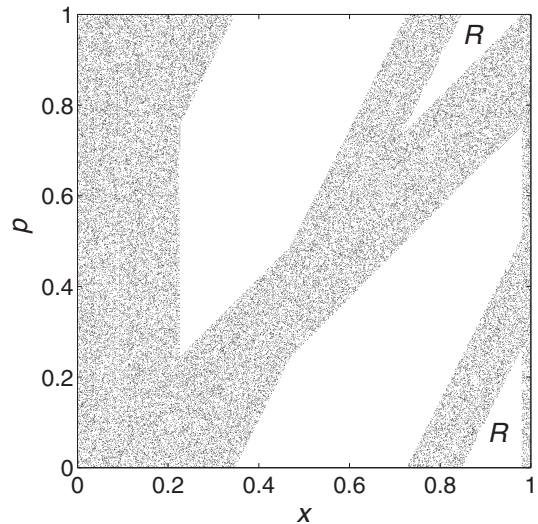Clearly, this will be always satisfied for $K > 2$ and sufficiently small b_1 and b_2 since $F(b_1) \approx (K - 2)/(K - 1)$ for $b_1 \ll 1$ in

FIG. 4. Global chaotic region for $K = 3$, $b_1 = 0.226$, and $b_2 = 0.02$. For these values of b_1 and b_2 only the right period-1 AMI exists (compare with Fig. 3).

Eq. (17); thus, both AMIs exist in the arbitrarily weak chaos regime. For $K = 3$, this case corresponds to the domain LR in Fig. 3.

(b) Only one AMI, say the right one R, exists (as, e.g., in Fig. 4) if

$$b_2 \geqslant F(b_1), \quad b_1 < F(b_2). \tag{19}$$

Similarly, if $b_2 < F(b_1)$ and $b_1 \geqslant F(b_2)$ only the left AMI L exists. For $K = 3$, this case corresponds to the domain R or L in Fig. 3.

(c) No AMIs exist if

$$b_2 \geqslant F(b_1), \quad b_1 \geqslant F(b_2). \tag{20}$$

It is easy to show from the expression for $F(b_1)$ in Eq. (17) (see also note [28]) that $F(b_1) \leqslant (K - 2)/(K - 1) - b_1$. One then gets from Eqs. (18)–(20) a simple necessary condition for the existence of at least one AMI:

$$b_1 + b_2 < \frac{K - 2}{K - 1}. \tag{21}$$

For the symmetric system ($b_1 = b_2$), the condition in Eq. (17) reads $b_1 < F(b_1)$, which can be significantly simplified:

$$b_1 < \frac{1}{2} - \frac{1}{K}. \tag{22}$$

It follows from the condition in Eq. (22) that no period-1 AMIs can exist if $b_1 = b_2 \geqslant 1/4$ for any value of K in the relevant interval of $2 \leqslant K < 4$. This is consistent with the known fact that bounding KAM tori exist for some K if $b_1 = b_2 = 1/4$ [27], which is apparently the only case of the map in Eq. (8) studied until now.

IV. RATCHET ACCELERATION FOR $K = 3$

In this section the ratchet acceleration A in the case of $K = 3$ will be calculated analytically in the framework of a plausible assumption (see below), supported by extensive numerical evidence and exact results. To use the sum rule in Eq. (6), we first identify the global chaotic region $\mathcal{C}$ in the basic periodicity torus $\mathbb{T}^2$. Let us denote by C the set of all iterates of the vertical strip B in Eq. (13) under $\bar{M}$, i.e., the map in Eq. (8) modulo $\mathbb{T}^2$ (see Sec. II):

$$C = \bigcup_{s = -\infty}^{\infty} \bar{M}^s B. \tag{23}$$

Exact results for the set in Eq. (23) are derived in Appendixes B–E. Here we note that orbits that never visit B (and thus also C) are all stable since they lie entirely within the middle interval in Eq. (9) where the linearized map DM has stability eigenvalues [Eq. (12)]. Thus the global chaotic region $\mathcal{C}$ must be entirely contained within C, in agreement with our expectation at the end of Sec. III B. Our extensive numerical studies indicate that C is indistinguishable from $\mathcal{C}$ [compare, e.g., Figs. 1(a) and 4 with Figs. 11 and 12 in Appendix C]. In fact, finite-time Lyapunov exponents of orbits starting from initial conditions covering B uniformly were all found to be strictly positive. We shall therefore assume in what follows that $\mathcal{C}$ precisely coincides with C. The rest of phase space outside $\mathcal{C}$ consists of no more than three stability regions [see, e.g.,

Figs. 1(a) and 4]: the left AMI L ($w = 1$), the right AMI R ($w = -1$), and a normal island ($w = 0$) lying between L and R. Using the sum rule in Eq. (6) with $v_j = w_j$ [since $m = 1$ in Eq. (5)], we then get a formula for the ratchet acceleration:

$$A = \frac{S_R - S_L}{S_C}. \tag{24}$$

Exact expressions for the areas S_L, S_R, and S_C are derived in Appendixes D and E using simple geometry [see Eqs. (D2), (D3), and (E2)–(E4) therein]. Inserting these expressions in the formula in Eq. (24), we obtain, after some algebra, explicit results for A in different cases.

(a) If both AMIs exist, i.e., the case in Eq. (18),

$$A = \frac{(b_1 - b_2)[1 - 3(b_1 + b_2)]}{2(2 - b_1 - b_2)(b_1 + b_2)}. \tag{25}$$

(b) If only one AMI, say the right one, exists, i.e., the case in Eq. (19),

$$A = \frac{(2 - 3b_2 - 3c)^2}{6(b_1 + b_2) - 6(b_1 + b_2)^2 + (3c - 3b_1 - 1)^2}. \tag{26}$$

(c) If no AMIs exist, i.e., the case in Eq. (20), $A = 0$, of course.

In general, the results in Eqs. (25) and (26) were found to agree very well with numerical calculations of A (see examples at the end of the following section). This is additional evidence for the validity of the basic assumption above concerning the chaotic region, $\mathcal{C} = C$.

V. MAXIMAL RATCHET ACCELERATION FOR ARBITRARILY WEAK CHAOS

In this section we show that the maximal ratchet acceleration A for $K = 3$ is attained in a limit $b_1, b_2 \to 0$ of arbitrarily weak chaos. In Fig. 5 we plot $|A|$ as function of b_1 and b_2 using
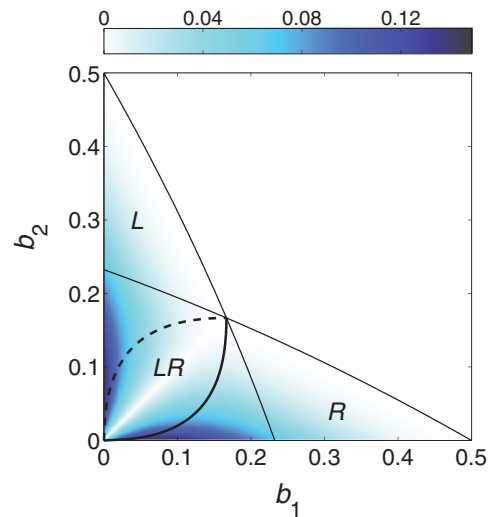

FIG. 5. (Color online) Pseudocolor plot of $|A|$ as a function of b_1 and b_2 for $K = 3$. The thin solid lines (defining the three domains L, R, and LR) are the same as those in Fig. 3. The thick solid line in domain LR is the maximal path [Eq. (27)] on which A is given by Eq. (28). The dashed line is the maximal path $b_2(b_1)$ [defined similarly to Eq. (27)] on which $A < 0$.
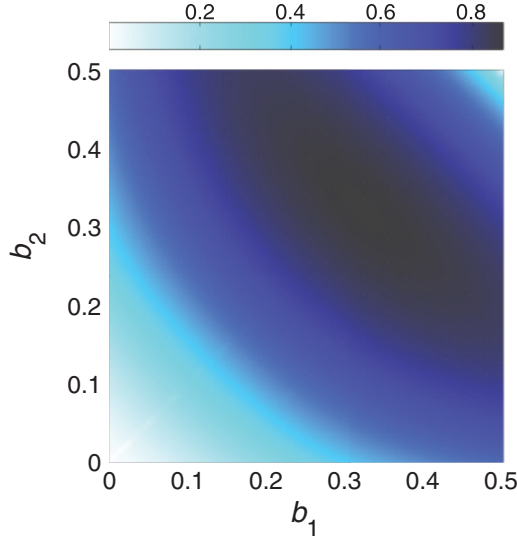
FIG. 6. (Color online) Pseudocolor plot of the Lyapunov exponent σ of the chaotic region as a function of b_1 and b_2 for $K = 3$.

the formulas in Eqs. (25) and (26) and $A(b_2,b_1) = -A(b_1,b_2)$. The Lyapunov exponent σ of the chaotic region as a function of b_1 and b_2 was calculated numerically with high accuracy and is plotted in Fig. 6. As one could expect, σ vanishes in the limit of $b_1,b_2 \to 0$, where the map in Eq. (8) tends to the ESM (see Sec. III B). It is clear from Fig. 5 that $|A|$ assumes its largest values in the parameter domain LR, where both AMIs exist. We shall therefore focus on this domain in which A is given by Eq. (25). We shall first calculate analytically the value of b_1 where $|A(b_1,b_2)|$ is maximal at fixed b_2; this will define a path $b_1(b_2)$ in the (b_1,b_2) plane [a path $b_2(b_1)$ can be similarly defined]. We then show that $|A(b_1,b_2)|$ is maximal on this path in the limit of $b_1,b_2 \to 0$. Let us take the partial derivative of the function in Eq. (25) with respect to b_1 and require that $\partial A/\partial b_1 = 0$. After a tedious but straightforward calculation, we find that the latter equation reduces to a quadratic one with the only positive root:

$$b_1(b_2) = \frac{2[5b_2(1 - b_2)]^{1/2} - b_2(7 - 6b_2)}{5 - 6b_2}. \qquad (27)$$

The path in Eq. (27) corresponds to the lower curve in Fig. 5, with $b_1 \geqslant b_2$. This curve starts at $b_1 = b_2 = 0$, with $b_1 \approx 2\sqrt{b_2/5}$ for $b_2 \ll 1$, and terminates at $b_1 = b_2 = 1/6$, on the boundary of the LR domain. For $b_2 \leqslant 1/6$, we find that $\partial^2 A/\partial b_1^2 < 0$ at the value of b_1 in Eq. (27), which thus corresponds to a local maximum. From Eqs. (25) and (27), the ratchet acceleration on the path in Eq. (27) is

$$A(b_2) = \frac{\{5 - 6[5b_2(1 - b_2)]^{1/2}\}^2}{20\{5 - 4b_2 - [5b_2(1 - b_2)]^{1/2}\}}. \qquad (28)$$

In the limit of $b_2 \to 0$ ($b_1 \approx 2\sqrt{b_2/5}$), we get, from Eq. (28),

$$\lim_{b_2 \to 0} A(b_2) = 1/4. \qquad (29)$$

After a simple but lengthy calculation we find that the function in Eq. (28) satisfies $\partial A/\partial b_2 < 0$ for $b_2 \leqslant 1/6$. Thus $A(b_2)$ decreases monotonically from $1/4$ (at $b_1 = b_2 = 0$) to 0 (at $b_1 = b_2 = 1/6$) on the path in Eq. (27). Since this path gives

the single extremum (a local maximum) of $A(b_1,b_2)$ for $b_1 \geqslant b_2$ at fixed b_2 and since $A(b_1,b_2) = 0$ for $b_1 = b_2$, we conclude that in the lower part ($b_1 \geqslant b_2$) of the LR domain $A(b_1,b_2) \geqslant 0$ and $A(b_1,b_2)$ assumes its maximal value of $1/4$ in the limit $b_1,b_2 \to 0$ of arbitrarily weak chaos on the path in Eq. (27).

Since $A(b_2,b_1) = -A(b_1,b_2)$, in the upper ($b_2 > b_1$) part of the LR domain $A(b_1,b_2) < 0$ and $A(b_1,b_2)$ assumes its maximal negative value of $-1/4$ in the limit of $b_1,b_2 \to 0$ on a path $b_2(b_1)$ (the dashed curve in Fig. 5), defined similarly to $b_1(b_2)$. The difference between the limiting values of $A(b_1,b_2)$ on the two paths reflects the discontinuity of the ESM, i.e., the map in Eq. (8) in the limit of $b_1,b_2 \to 0$. In general, $|A(b_1,b_2)|$ can assume in this limit all values $< 1/4$ on other, nonmaximal paths. For example, on the straight-line path $b_1 = b_2/a$, where a is some arbitrary constant, we find from Eq. (25) that

$$\lim_{b_2 \to 0} A(b_2) = \frac{(1 - a)}{4(1 + a)}. \qquad (30)$$

We remark that the path in Eq. (27) is tangent to the b_1 axis at $b_1 = b_2 = 0$ since $b_1 \approx 2\sqrt{b_2/5}$ for $b_2 \ll 1$. Similarly, the second maximal path $b_2(b_1)$ is tangent to the b_2 axis in this limit. Thus, as expected, the maximal value of $|A| = 1/4$ is associated with the largest possible asymmetry, $b_1/b_2 = \infty$ or $b_2/b_1 = \infty$ [$a = 0$ or $a = \infty$ in Eq. (30)].

Figures 7 and 8 show plots of A versus the Lyapunov exponent σ for small b_2 on both the maximal path in Eq. (27) and the path $b_1 = 3b_2$. We see in both plots excellent agreement between the values of A calculated numerically and those calculated from the formulas in Eqs. (25), (26), and (28).
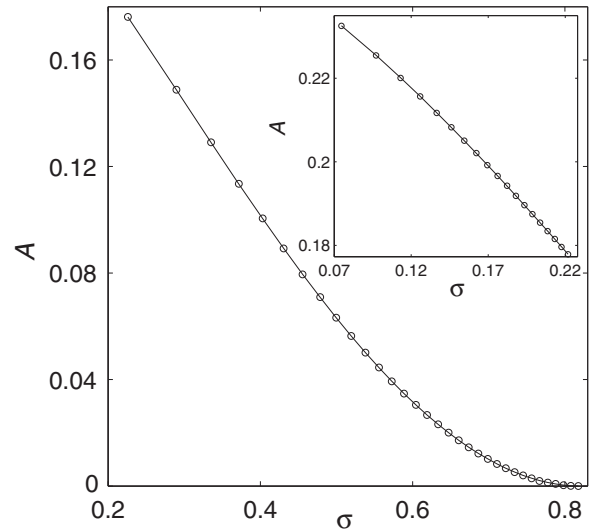

FIG. 7. Circles represent numerical results for A versus the Lyapunov exponent σ on the maximal path in Eq. (27) with b_2 distributed uniformly on the interval $0.005 \leqslant b_2 \leqslant 0.165$; these results were obtained by averaging $(p_n - p_0)/n$ ($n = 120\,000$) over an ensemble of 10^4 initial conditions (x_0, p_0) in the chaotic region, i.e., all having positive finite-time Lyapunov exponents. The solid line plots the analytical result in Eq. (28). The inset shows the continuation of the main plot to smaller values of b_2, distributed uniformly on the interval $0.000\,25 \leqslant b_2 \leqslant 0.004\,75$. In this interval of very weak chaos, A is close to its maximal value of $1/4$ [see Eq. (29)].
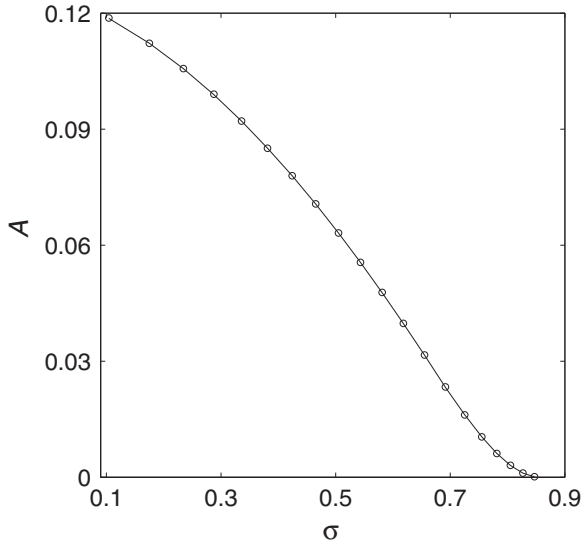
FIG. 8. Circles represent numerical results for A versus σ on the path $b_1 = 3b_2$ with b_2 distributed uniformly on the interval $0.005 \leqslant b_2 \leqslant 0.1$ [this path crosses both domains LR and R (see Fig. 3)]; these results were obtained as described in the caption of Fig. 7. The solid line plots the analytical results from the formulas in Eqs. (25) and (26). For small σ, $A \approx 0.12$, close to the predicted limiting value of $A = 0.125$ from Eq. (30) ($a = 1/3$).

VI. CONCLUSIONS

In this paper we have introduced a realistic non-KAM system exhibiting, in weak-chaos regimes, the most significant Hamiltonian ratchet effect of directed acceleration. The system, defined by the generalized standard map in Eq. (8) with Eq. (9), may be viewed as a perturbed ESM with a perturbation that removes the ESM discontinuity. Thus the global weak chaos featured by the system may be generally considered as a perturbed global pseudochaos. Our main exact result is that for $K = 3$ the maximal ratchet acceleration A is attained precisely in a limit $b_1, b_2 \to 0$ of arbitrarily weak chaos with an infinite asymmetry parameter ($b_1/b_2 = \infty$ or $b_2/b_1 = \infty$). Despite this, the limiting system is interestingly the completely symmetric ESM (see phase spaces in Fig. 2). By continuity considerations, one expects that at least for values of K sufficiently close to $K = 3$ one should again observe a significant increase of the absolute value $|A|$ of the acceleration as the chaos strength decreases. We have verified this numerically in parameter regimes where good accuracy could be achieved within the limitations of our available computational resources. An example is shown in Fig. 9.

Our main result that the strongest Hamiltonian ratchet effect can arise in a limit of arbitrarily weak chaos apparently has no analog in ordinary ratchets if chaos is viewed as the deterministic counterpart of random noise. In fact, a sufficiently high level of noise is essential for the functioning of ordinary ratchets or Brownian motors [17,18]. Actually, it was recently shown that for a Lévy ratchet the current decreases algebraically with the noise level [18], in clear contrast with our results.

The quantized version of our non-KAM system may be experimentally realized using, e.g., optical analogs as proposed in Ref. [26] and is expected to exhibit, in general, a rich variety
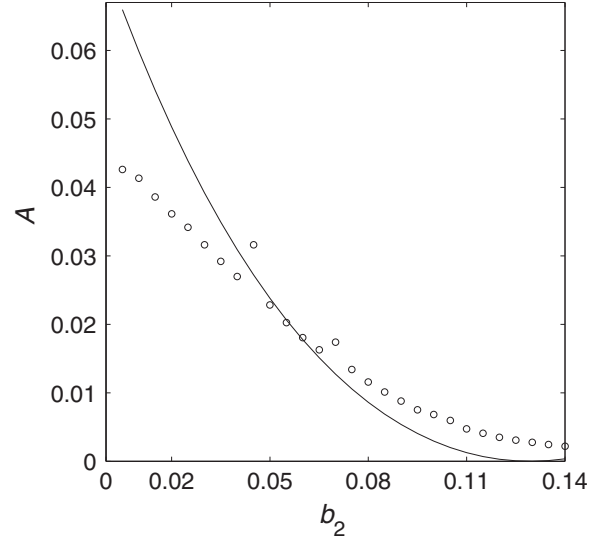

FIG. 9. Circles represent numerical values of A (obtained as described in the caption of Fig. 7) for $K = 2.99$ on the path $b_1 = 0.25$ and $0.005 \leqslant b_2 \leqslant 0.14$; this path lies entirely in domain R (see Fig. 3 for the nearby value of $K = 3$). The Lyapunov exponent on the path varies in the interval $0.4787 < \sigma < 0.8326$. The solid line plots the analytical results from the formula in Eq. (26) for $K = 3$.

of quantum phenomena, including the quantum signatures of the weak-chaos ratchet acceleration. The study of these phenomena is planned to be the subject of future work.

APPENDIX A

We derive here Eqs. (10). First, continuity of the function in Eq. (9) at $x = b_1$ and $1 - b_2$ implies that

$$l_1 b_1 = c - b_1, \quad l_2 b_2 = 1 - b_2 - c. \tag{A1}$$

Then, using Eqs. (9) and (A1) in the ratchet condition $\int_0^1 f(x)dx = 0$, we find that

$$\int_0^1 f(x)\,dx = c - \frac{b_1}{2}c + \frac{b_2}{2}(1 - c) - \frac{1}{2} = 0,$$

yielding the expression for c in Eqs. (10). After inserting this expression in Eqs. (A1), we get the expressions for l_1 and l_2 in Eqs. (10).

APPENDIX B: REGION C FOR $K = 3$

In this Appendix and in the following ones, we derive, for $K = 3$, exact results for the region C in Eq. (23). As mentioned in Sec. IV, several arguments and extensive numerical evidence indicate that C coincides with the chaotic region $\mathcal{C}$ for $K = 3$. We show here that one has the simple relation

$$C = C' = B \cup \bar{M}B \cup \bar{M}^2 B. \tag{B1}$$

To show this, we first denote

$$\bar{B}^{(1)} = \bar{M}B - B \cap \bar{M}B, \tag{B2}$$

$$\bar{B}^{(2)} = \bar{M}\bar{B}^{(1)} - B \cap \bar{M}\bar{B}^{(1)}. \tag{B3}$$

We derive below the relation

$$\bar{M}\bar{B}^{(2)} \subseteq B. \tag{B4}$$

Then, from the definition of C' in Eq. (B1) and from Eqs. (B2)–(B4) it follows that

$$\bar{M}C' \subseteq C'. \tag{B5}$$

Equation (B5) and the fact that $\bar{M}$ is area preserving imply that $\bar{M}C' = C'$ or $\bar{M}^{-1}C' = C'$. Thus $C' = \bar{M}^s B \cup \bar{M}^{s+1} B \cup \bar{M}^{s+2} B$ for all integers s, which is possible only if C' is equal to C in Eq. (23). Relation (B1) is thus proven.

To derive Eq. (B4) we start by obtaining an explicit expression for $\bar{B}^{(1)}$ in Eq. (B2). For $K = 3$, the iterate of any initial condition (x_0, p_0) under $\bar{M}$ satisfies $p_1 = x_1 - x_0 \bmod(1)$, $x_1 = x_0 + p_0 + 3f(x_0) \bmod(1)$. Clearly, when p_0 varies in $[0,1)$ at fixed x_0, x_1 varies in the whole interval $[0,1)$. Then, taking (x_0, p_0) in B and using Eqs. (13) and (B2), we get

$$\bar{M}B = \{(x,p) | 0 \leqslant x < 1, \quad x - b_1 \leqslant p \leqslant x + b_2\} \bmod(\mathbb{T}^2), \tag{B6}$$

$$\bar{B}^{(1)} = \{(x,p) | b_1 < x < 1 - b_2, \quad x - b_1 \leqslant p \leqslant x + b_2\}. \tag{B7}$$

The region in Eq. (B7) is a strip (parallelogram) of slope 1, shown in Fig. 10(b) and corresponding to the strip B in Fig. 10(a). Next we determine the region

$$B^{(2)} = \bar{M}\bar{B}^{(1)}. \tag{B8}$$

The second iterate (x_2, p_2) of (x_0, p_0) under $\bar{M}$, with $(x_0, p_0) \in B$ and $(x_1, p_1) \in \bar{B}^{(1)}$, is given by

$$p_2 = p_1 - 3(x_1 - c) \bmod(1)$$
$$= -2x_1 - x_0 + 3c \bmod(1), \tag{B9}$$

$$x_2 = x_1 + p_2 \bmod(1) = -2x_1 + p_1 + 3c \bmod(1). \tag{B10}$$

From Eq. (B9) and the first equality of Eq. (B10) we find that

$$p_2 = 2x_2 + x_0 - 3c \bmod(1). \tag{B11}$$

Equation (B11) and the second equality of Eq. (B10) imply that the region in Eq. (B8) is the following set of phase-space points:

$$B^{(2)} = \{(x,p)\}$$
$$: \begin{cases} x = -2x_1 + p_1 + 3c \bmod(1), & (x_1, p_1) \in \bar{B}^{(1)}, \\ p = 2x + x_0 - 3c \bmod(1), & -b_2 \leqslant x_0 \leqslant b_1. \end{cases} \tag{B12}$$

The region in Eq. (B12) is clearly a parallelogram of slope 2 folded into $\mathbb{T}^2$, as shown in Fig. 10(c). The region $\bar{B}^{(2)}$ in Eq. (B3) is given by Eq. (B12) with x restricted to the
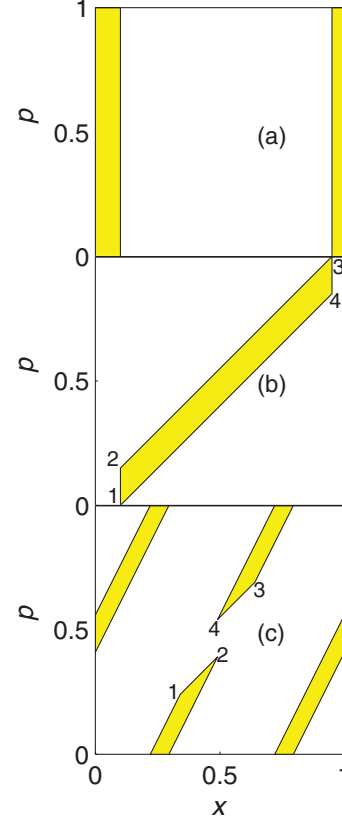

FIG. 10. (Color online) Shown, for $K = 3$, $b_1 = 0.1$, and $b_2 = 0.05$, are (a) the strip B [see Eq. (13)], (b) the region $\bar{B}^{(1)}$ [see Eq. (B2) or (B7)], and (c) the region $B^{(2)}$ [see Eq. (B8) or (B12)].

interval $b_1 < x < 1 - b_2$. Then, using also Eq. (B11), we get, for $(x_0, p_0) \in B$ and $(x_2, p_2) \in \bar{B}^{(2)}$,

$$\bar{M}\bar{B}^{(2)} = \{(x,p)\}$$
$$: \begin{cases} p = p_2 - 3(x_2 - c) \bmod(1) = x_0 - x_2 \bmod(1), \\ x = x_2 + p \bmod(1) = x_0 \bmod(1). \end{cases} \tag{B13}$$

The result in Eqs. (B13) and Eq. (13) imply Eq. (B4).

APPENDIX C: AMIs AND THE SHAPE OF C

We study here the shape of the region C for $K = 3$ in several cases. Let us write Eq. (B1) as $C = C' = B \cup \bar{B}^{(1)} \cup B^{(2)}$, i.e., the union of the three sets in Fig. 10. This union is shown in Fig. 11, exhibiting a case in which both the L and R AMIs exist (see Secs. III C and IV). For values of b_1 and/or b_2 larger than those in Figs. 10 and 11, there may exist only one AMI or no AMIs (see Fig. 3). A case of C for which only the R AMI exists is shown in Fig. 12 and is clearly different from that in Fig. 11. We show below that the existence of AMIs and the shape of C in different cases depend on the location of the vertices $(x^{(j)}, p^{(j)})$ $(j = 1,2,3,4)$ of the parallelogram in Eq. (B12) [shown in Fig. 10(c)] relative to the strip B. Because of Eq. (B8), one has $(x^{(j)}, p^{(j)}) = \bar{M}(\bar{x}^{(j)}, \bar{p}^{(j)})$, where $(\bar{x}^{(j)}, \bar{p}^{(j)})$ $(j = 1,2,3,4)$ are the vertices of the parallelogram
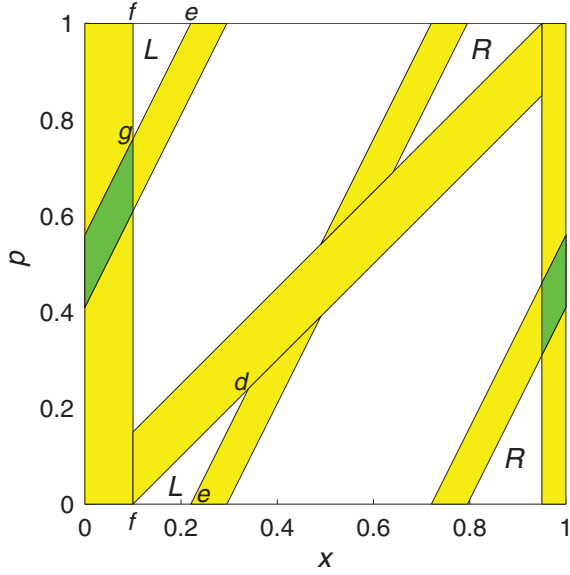
FIG. 11. (Color online) Region C, given by the union of the three regions shown in Fig. 10, with overlaps indicated by green (dark gray). Both AMIs L and R exist in this case. See the text for more details.

in Eq. (B7), shown in Fig. 10(b). Clearly,

$$(\bar{x}^{(1)}, \bar{p}^{(1)}) = (b_1, 0), \quad (\bar{x}^{(2)}, \bar{p}^{(2)}) = (b_1, b),$$
$$(\bar{x}^{(3)}, \bar{p}^{(3)}) = (1 - b_2, 1), \quad (\bar{x}^{(4)}, \bar{p}^{(4)}) = (1 - b_2, 1 - b),$$
(C1)

where $b = b_1 + b_2$. To derive explicit expressions for $(x^{(j)}, p^{(j)}) = \bar{M}(\bar{x}^{(j)}, \bar{p}^{(j)})$, one has to properly determine the additive integers from the modulo operations in $\bar{M}$ so that
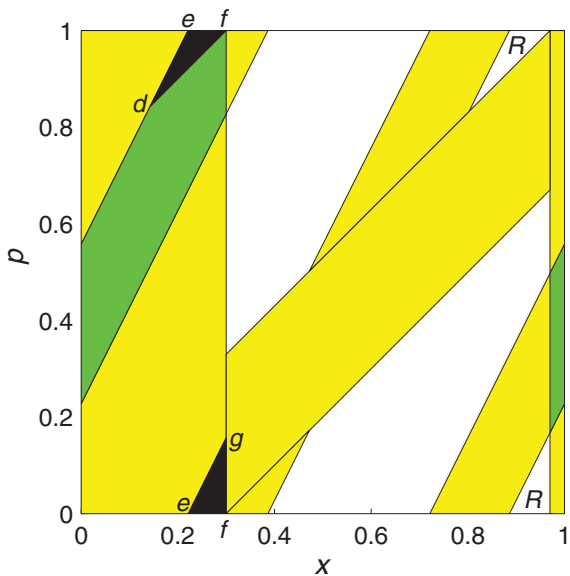

FIG. 12. (Color online) Region $C = B \cup \bar{B}^{(1)} \cup \bar{B}^{(2)}$ for $K = 3$, $b_1 = 0.3$, and $b_2 = 0.03$, with overlaps indicated by green (dark gray). Only the R AMI exists in this case. See the text for more details.

$(x^{(j)}, p^{(j)})$ will lie within the basic torus $\mathbb{T}^2$. We find that the values of $x^{(j)}$ are

$$x^{(1)} = 3c - 2b_1 - 1, \quad x^{(2)} = x^{(4)} = x^{(1)} + b,$$
$$x^{(3)} = x^{(1)} + 2b,$$
(C2)

indeed satisfying $0 < x^{(j)} < 1$ in the relevant cases in which at least one AMI exists. In fact, in these cases one has $b < 0.5$ [from Eq. (21) with $K = 3$] and the latter inequality implies by simple algebra that the smallest value of $x^{(j)}$ in Eqs. (C2), i.e., $x^{(1)}$, satisfies $x^{(1)} > 0$ while the largest value ($x^{(3)}$) satisfies $x^{(3)} < 1$. In addition, it is clear from Figs. 10–12 that the R AMI exists only if $x^{(3)} < 1 - b_2$ (vertex 3 is outside B); it is easy to show that the latter inequality is indeed equivalent to the existence condition $b_1 < F(b_2)$ for the R AMI, derived in Sec. III C. Similarly, the L AMI exists only if $x^{(1)} > b_1$ (vertex 1 is outside B), which can be easily shown to be equivalent to the existence condition in Eq. (17). Thus, when both AMIs exist, $b_1 < x^{(j)} < 1 - b_2$ ($j = 1,2,3,4$).

To determine the values of $p^{(j)}$, we first notice that the vertices $(x^{(j)}, p^{(j)})$ must touch the boundaries of the region in Eq. (B6); this is because the vertices in Eq. (C1), shown in Fig. 10(b), obviously touch the boundaries of the strip B in Fig. 10(a) and $(x^{(j)}, p^{(j)}) = \bar{M}(\bar{x}^{(j)}, \bar{p}^{(j)})$. Then, in the case that both AMIs exist, i.e., $b_1 < x^{(j)} < 1 - b_2$ (see above), $(x^{(j)}, p^{(j)})$ touch the boundaries $p = x - b_1$ and $p = x + b_2$ of the parallelogram in Eq. (B7) [see Figs. 10(b), 10(c), and 11], so that

$$p^{(1,2)} = x^{(1,2)} - b_1, \quad p^{(3,4)} = x^{(3,4)} + b_2.$$
(C3)

Assume now that only the R AMI exists, as in Fig. 12. Then $x^{(1)} \leqslant b_1$ (from above), i.e., vertex 1 (the point d in Figs. 11 and 12) lies within the left part of strip B, on the boundary of the region in Eq. (B6), given by $p = x - b_1 \mod(1)$; thus, for $x^{(1)} < b_1$ (as in Fig. 12), $p^{(1)}$ in Eq. (C3) must be replaced by $x^{(1)} - b_1 + 1$ while $p^{(j)}$ for $j > 1$ remains unchanged. Similarly, when only the L AMI exists, vertex 3 lies within the right part of strip B, on the boundary of the region in Eq. (B6), given by $p = x + b_2 \mod(1)$; for $x^{(3)} > 1 - b_2$, $p^{(3)}$ in Eq. (C3) must be replaced by $x^{(3)} + b_2 - 1$.

APPENDIX D: AREAS OF AMIs

Consider the L AMI in Fig. 11. This is the triangle dfg on the torus $\mathbb{T}^2$, composed of two triangles def and efg. The point d is vertex 1 in Fig. 10(c) and the segment de is part of the upper boundary of the region in Eq. (B12). This boundary is a line of slope 2 passing through vertex 1:

$$p - p^{(1)} = 2(x - x^{(1)}).$$
(D1)

Then, since $p_e = 0$, we get from Eqs. (C2)–(D1) that $x_e = (3c - b_1 - 1)/2$. Also, $x_f = b_1$ and $p_f = 0$. The point g, with $x_g = b_1$, lies on the line in Eq. (D1) with $p^{(1)}$ replaced by $p^{(1)} + 1$. Thus $p_g = 2 + 3b_1 - 3c$. The area of the L AMI is therefore

$$S_L = S_{def} + S_{efg} = \tfrac{1}{2}(x_e - x_f)[p^{(1)} + (1 - p_g)]$$
$$= \tfrac{1}{2}(3c - 3b_1 - 1)^2.$$
(D2)

By symmetry arguments, the area of the R AMI is obtained from Eq. (D2) by inserting the expression for c from Eqs. (10) and performing the exchange $b_1 \leftrightarrow b_2$. We get

$$S_R = \tfrac{1}{2}(2 - 3b_2 - 3c)^2. \tag{D3}$$

APPENDIX E: AREA OF C

The area of C can be calculated starting from the relation $C = B \cup \bar{B}^{(1)} \cup B^{(2)}$ (see above), where $\bar{B}^{(1)}$ and B do not overlap. Then, because of Eqs. (B2) and (B8), $B^{(2)}$ also does not overlap with $\bar{B}^{(1)}$. However, it may overlap with B. The area of C is thus given by

$$S_C = S_B + S_{\bar{B}^{(1)}} + S_{B^{(2)}} - S_{B \cap B^{(2)}}. \tag{E1}$$

From Eq. (13), $S_B = b$, where $b = b_1 + b_2$. The region $\bar{B}^{(1)}$ in Eq. (B7) is a parallelogram with basis b (in the p direction) and height $1 - b$ (in the x direction) (see also Figs. 11 and 12). Thus $S_{\bar{B}^{(1)}} = b(1 - b)$. From Eq. (B8) and the fact that $\bar{M}$ is area preserving, it follows that $S_{B^{(2)}} = S_{\bar{B}^{(1)}}$. Finally, concerning the overlap $B \cap B^{(2)}$, we consider first the case that both AMIs exist (see Fig. 11). In this case, $B \cap B^{(2)}$ consists of the green (dark gray) regions in Fig. 11. These are two parallelograms having heights b_1 and b_2 (in the x direction) and basis b, i.e.,

the width of the region in Eq. (B12) in the p direction. Thus $S_{B \cap B^{(2)}} = b^2$. The area in Eq. (E1) is therefore

$$S_C = 3(b_1 + b_2) - 3(b_1 + b_2)^2. \tag{E2}$$

Consider now the case that only one AMI exists, say the R AMI as in Fig. 12. In this case, as explained at the end of Appendix C, the point d, i.e., the vertex 1 of region $B^{(2)}$, lies inside the left part of strip B, on the boundary of the region in Eq. (B6). This means that the black triangles def and efg in Fig. 12 are not included in the region $B^{(2)}$ or $B \cap B^{(2)}$ but they are actually part of the region (B6). Thus, to calculate $S_{B \cap B^{(2)}}$ one must subtract from b^2 (the value of $S_{B \cap B^{(2)}}$ in the previous case) the areas of def and efg. The area in Eq. (E1) is then obtained by adding $S_{def} + S_{efg}$ to the expression in Eq. (E2). By comparing Fig. 12 with Fig. 11, it is clear that the areas S_{def} and S_{efg} can be calculated precisely as in Appendix D and $S_{def} + S_{efg}$ is given again by the formula in Eq. (D2). Therefore, the area in Eq. (E2) increases precisely by an amount equal to the area in Eq. (D2) of the missing L AMI:

$$S_C = 3(b_1 + b_2) - 3(b_1 + b_2)^2 + (3c - 3b_1 - 1)^2/2. \tag{E3}$$

Similarly, when only the L AMI exists, one must add the area in Eq. (D3) to Eq. (E2):

$$S_C = 3(b_1 + b_2) - 3(b_1 + b_2)^2 + (2 - 3b_2 - 3c)^2/2. \tag{E4}$$

[1] S. Flach, O. Yevtushenko, and Y. Zolotaryuk, Phys. Rev. Lett. **84**, 2358 (2000).

[2] T. Dittrich, R. Ketzmerick, M.-F. Otto, and H. Schanz, Ann. Phys. (Leipzig) **9**, 755 (2000).

[3] H. Schanz, M.-F. Otto, R. Ketzmerick, and T. Dittrich, Phys. Rev. Lett. **87**, 070601 (2001); H. Schanz, T. Dittrich, and R. Ketzmerick, Phys. Rev. E **71**, 026228 (2005).

[4] S. Denisov and S. Flach, Phys. Rev. E **64**, 056236 (2001); S. Denisov, J. Klafter, M. Urbakh, and S. Flach, Physica D **170**, 131 (2002); S. Denisov, S. Flach, A. A. Ovchinnikov, O. Yevtushenko, and Y. Zolotaryuk, Phys. Rev. E **66**, 041104 (2002).

[5] T. Cheon, P. Exner, and P. Seba, J. Phys. Soc. Jpn. **72**, 1087 (2003).

[6] J. Gong and P. Brumer, Phys. Rev. E **70**, 016202 (2004).

[7] T. S. Monteiro, P. A. Dando, N. A. C. Hutchings, and M. R. Isherwood, Phys. Rev. Lett. **89**, 194102 (2002); N. A. C. Hutchings, M. R. Isherwood, T. Jonckheere, and T. S. Monteiro, Phys. Rev. E **70**, 036205 (2004); G. Hur, C. E. Creffield, P. H. Jones, and T. S. Monteiro, Phys. Rev. A **72**, 013403 (2005).

[8] S. Denisov, L. Morales-Molina, S. Flach, and P. Hänggi, Phys. Rev. A **75**, 063424 (2007).

[9] E. Lundh and M. Wallin, Phys. Rev. Lett. **94**, 110603 (2005); A. Kenfack, J. Gong, and A. K. Pattanayak, *ibid.* **100**, 044104 (2008).

[10] I. Dana and V. Roitberg, Phys. Rev. E **76**, 015201(R) (2007); M. Sadgrove and S. Wimberger, New J. Phys. **11**, 083027 (2009).

[11] I. Dana, Phys. Rev. E **81**, 036210 (2010).

[12] J. Gong and P. Brumer, Phys. Rev. Lett. **97**, 240602 (2006); J. Pelc, J. Gong, and P. Brumer, Phys. Rev. E **79**, 066207 (2009), and references cited therein.

[13] P. H. Jones, M. Goonasekera, D. R. Meacher, T. Jonckheere, and T. S. Monteiro, Phys. Rev. Lett. **98**, 073002 (2007).

[14] M. Sadgrove, M. Horikoshi, T. Sekimura, and K. Nakagawa, Phys. Rev. Lett. **99**, 043002 (2007).

[15] I. Dana, V. Ramareddy, I. Talukdar, and G. S. Summy, Phys. Rev. Lett. **100**, 024103 (2008); I. Dana, V. B. Roitberg, V. Ramareddy, I. Talukdar, and G. S. Summy, Int. J. Bifurcation Chaos **20**, 255 (2010).

[16] T. Salger *et al.*, Science **326**, 1241 (2009).

[17] P. Hänggi and F. Marchesoni, Rev. Mod. Phys. **81**, 387 (2009), and references cited therein.

[18] I. Pavlyukevich, B. Dybiec, A. V. Chechkin, and I. M. Sokolov, e-print arXiv:1008.4246, and references cited therein.

[19] R. Ishizaki, T. Horita, T. Kobayashi, and H. Mori, Prog. Theor. Phys. **85**, 1013 (1991).

[20] G. M. Zaslavsky, R. Z. Sagdeev, D. A. Usikov, and A. A. Chernikov, *Weak Chaos and Quasi-Regular Patterns* (Cambridge University Press, Cambridge, 1991), and references cited therein.

[21] P. Ashwin, Phys. Lett. A **232**, 409 (1997).

[22] G. M. Zaslavsky, Phys. Rep. **371**, 461 (2002), and references cited therein.

[23] K. Koupstov, J. H. Lowenstein, and F. Vivaldi, Nonlinearity **15**, 1795 (2002); J. H. Lowenstein, K. L. Kouptsov, and F. Vivaldi, *ibid.* **17**, 371 (2004).

[24] I. Dana, Phys. Rev. E **69**, 016212 (2004).

[25] G. Benenti, G. Casati, S. Montangero, and D. L. Shepelyansky, Phys. Rev. Lett. **87**, 227901 (2001); Eur. Phys. J. D **22**, 285 (2003); S. Bettelli and D. L. Shepelyansky, Phys. Rev. A **67**, 054303 (2003).

[26] J. Krug, Phys. Rev. Lett. **59**, 2133 (1987); M. Schwägerl and J. Krug, Physica D **52**, 143 (1991).

[27] M. Wojtkowski, Commun. Math. Phys. **80**, 453 (1981); S. Bullett, *ibid.* **107**, 241 (1986); R. Scharf and B. Sundaram, Phys. Rev. A **45**, 3615 (1992); **46**, 3164 (1992).

[28] One can also easily show that in the condition in Eq. (17) (with $2 \leqslant K < 4$) one must have $b_1 < b_1^{(-)}$, where $b_1^{(-)} = (2K - 1 - \sqrt{4K + 1})/2K$ is the smallest root of $F(b_1) = 0$ and $F(b_1)$ decreases monotonically from $F(b_1 = 0) = (K - 2)/(K - 1)$ to $F(b_1 = b_1^{(-)}) = 0$. In addition, $b_1^{(-)} < b_1^{(0)}$, where $b_1^{(0)} = (K - 1)/K$ is the value of b_1 at which the denominator of $F(b_1)$ vanishes. Thus this denominator is always positive in the condition in Eq. (17). Similar results hold for analogous conditions in Sec. III C.